

UNIVERSITY OF SOUTHAMPTON

SEPTEMBER 2017

FACULTY OF NATURAL AND ENVIRONMENTAL
SCIENCES

OCEAN AND EARTH SCIENCE

**ESTIMATING THE DEEP OVERTURNING
TRANSPORT VARIABILITY AT 26°N USING
BOTTOM PRESSURE RECORDERS.**

Emma Worthington

A dissertation submitted in partial fulfilment of the requirements
for the degree of M.Sc. (Oceanography) by instructional course.

As the nominated University supervisor of the M.Sc. project by Emma Worthington, I confirm that I have had the opportunity to comment on earlier drafts of the report prior to submission of the dissertation for consideration of the award of M.Sc. (Oceanography).

Signed:

Supervisor's name: Dr. Eleanor Frajka-Williams

ACKNOWLEDGEMENT

I would like to thank my supervisors, Dr Eleanor Frajka-Williams and Dr Gerard McCarthy for their help and patience, my husband Pete for his endless support, and my classmates and lecturers on the M.Sc. Oceanography course 2016/17 for making this such a memorable year. Thank you.

Emma Worthington

Contents

1	Introduction	6
2	Background - AMOC transport calculations	8
3	Methods	9
3.1	Data	9
3.2	Removal of drift from bottom pressure data	11
3.3	Estimation of external transport variability	13
4	Results	18
4.1	Correlation between external transport and hypsometric compensation	18
4.2	Evaluation of using GRACE data	21
4.3	Evaluation of including mid-Atlantic ridge transport	25
4.4	Trend over 10 years	27
5	Discussion	28
6	Conclusions	31

Abstract

The Atlantic meridional overturning circulation (AMOC) carries almost 90% of the approximately 1.3 PW of heat carried poleward by the North Atlantic. The RAPID mooring array at 26°N in the Atlantic has been monitoring the AMOC since 2004, and its measurements suggest that the AMOC is declining in strength. Most of this decline is due to a weakening of the deep southward return flow. When AMOC transport is estimated, the barotropic transport component is not determined from measurements, but is a residual added to the baroclinic and Ekman transports and the Gulf Stream to ensure a zero net flow across the section. This approach was validated using the first year of RAPID data by estimating AMOC transport with the barotropic transport component directly derived from in-situ bottom pressure (BP) measurements, and finding good agreement with the residual method AMOC estimate. This study will use over a decade of RAPID BP data to estimate barotropic transport at 26°N.

BP sensor records commonly show low frequency instrument drift, but the standard method of removal also removes other long period signals. This study used over 10 years of bottom pressure data from both the RAPID array and the Gravity Recovery and Climate Experiment (GRACE) satellite mission, with the GRACE ocean bottom pressure (OBP) data used to remove the instrument drift from the RAPID array BP sensor records, leaving low-frequency signals intact. The GRACE-adjusted in-situ BP data were then used to estimate the barotropic transport variability at 26°N.

The detrended barotropic transport estimated from GRACE-adjusted, in-situ BP data correlated well ($r = 0.66$, $p < 0.01$) with the residual calculated during the RAPID AMOC calculation, and the two time series were coherent and in-phase for most periods from 10 to 180 days and longer than one year. However when the time series were not detrended, the 10-year trends were in opposition, with the GRACE-adjusted, in-situ BP-derived barotropic transport showing a strengthening southward flow in contrast to the weakening southward hypsometric compensation. In conclusion, using GRACE data to remove instrument drift from in-situ BP sensors appears effective, and the transport derived from the adjusted BP data provides independent verification for the RAPID AMOC calculations. However the GRACE data may itself contain low-frequency signals that are not removed during processing and cause the observed trend.

1 Introduction

Over a decade of measurements by the Rapid Climate Change (RAPID¹) mooring array at 26°N in the Atlantic suggest that the Atlantic meridional overturning circulation (AMOC) is declining in strength, and that most of this decline is due to a weakening of the deep return flow, which has shown a reduction of 7% per year between 2004 and 2012 (Smeed et al. 2014). The AMOC carries almost 90% of the approximately 1.3 PW of heat carried poleward by the North Atlantic, and the AMOC and heat transport are highly correlated (Johns et al. 2011). Since most of the heat carried by the upper limb of the AMOC is lost to the atmosphere as it moves poleward, it plays a vital role in maintaining the milder climate of North-West Europe (Rhines et al. 2008), and a weakening of the AMOC is likely to affect this. Global climate models simulating an AMOC slowdown show widespread cooling in North-West Europe and the North Atlantic, together with changes to precipitation patterns and more winter storms (Jackson et al. 2015).

Bottom pressure sensors are deployed as part of the RAPID array, however BP is not used to determine barotropic transport in the RAPID project's AMOC calculation (detailed in section 2). One reason is that in-situ measurements of bottom pressure at depth are subject to instrument drift, which introduces errors on longer timescales (greater than half the deployment period). Watts & Kontoyiannis (1990) examined the performance of fourteen commonly-used pressure sensors deployed at around 4000 m for 3 to 12 months in the Gulf Stream region. They found that instrument drift could be equivalent to as much as several centimetres of water height, compared to typical ocean pressure signals of around 1 cm, and that the drift varied in magnitude and direction even between the same sensor type. Instrument drift is typically exponential at the beginning of the record, combined with a linear drift throughout (Johns et al. 2005). The drift is usually removed by applying an exponential-linear curve whose parameters are determined from a least-squares fit of empirical data, however the removal does not distinguish between instrument drift and any true low-frequency signal (i.e., with a period longer than the record length) which will subsequently be lost. This study will instead use OBP data from the Gravity Recovery and Climate Experiment (GRACE) satellite mission to constrain the

¹Includes RAPID-AMOC, RAPID-MOCHA (Meridional Overturning and Heat-flux Array) and RAPID-WATCH projects (<http://www.rapid.ac.uk>).

instrument drift in the in-situ BP measurements, which should preserve low-frequency signals. GRACE is a joint U.S./German satellite mission that was launched on 17 March 2002. Its twin satellites orbit 220 km apart at an altitude of around 400 km, and detect changes in gravity which, over short timescales, are due to the movement of water at or just below the earth's surface. The data are processed by three different centres; the Centre for Space Research, University of Texas (CSR), GeoForschungsZentrum, Potsdam (GFZ), and the Jet Propulsion Laboratory, Pasadena (JPL), which each use different algorithms to process the data. The JPL Release-05 (RL05) produces global, monthly gravity fields within 'mascons', or mass concentration blocks, which are equal-area 3° spherical-cap cells. The ocean bottom pressures are reported as equivalent water thickness in centimetres. Apart from the coarse resolution, issues can be caused by 'leakage' due to land hydrography where a single mascon covers both land and ocean, or where a single mascon covers significantly different depths, making resolving the different bottom pressures impossible. Noise levels can also be high, although the latest RL05 dataset has an improved signal-to-noise ratio (Chambers & Bonin 2012).

Several studies have evaluated GRACE bottom pressure data against both ocean models (Bingham & Hughes 2008) and observations (Park et al. 2008, Landerer et al. 2015). The study by Park et al. (2008) compared GRACE Release-04 (RL04) bottom pressure data with sensor measurements from the Kuroshio Extension System Study (KESS), which was an array of 46 sensors over a 600 km^2 area off the east coast of Japan. The spatially-averaged, monthly-mean sensor data showed strong correlation with the GRACE bottom pressure data, particularly for the JPL and CSR datasets. The correlation between individual sensor and GRACE bottom pressures was strongly dependent on eddy kinetic energy (EKE), with low (high) correlation for sites with high (low) EKE. Landerer et al. (2015) made estimates of the deep (3000–5000 m) transport variability at 26°N using monthly GRACE OBP anomalies derived from the JPL Release-05 (RL05) mascon grid. This deep transport, called the Lower North Atlantic Deep Water (LNADW), is part of the southward return flow of the AMOC and correlates strongly with total AMOC transport variability. They found that their transport estimates correlated well ($r = 0.69$) with AMOC transport data from the RAPID project between 2004 and 2014 after detrending and low-pass filtering.

This study aims to extend the work done by Kanzow et al. (2007) by using the full 13-year

time series of RAPID bottom pressure data to estimate the external (also called the depth-independent or barotropic) transport (T_{EXT}) variability. The instrument drift in the in-situ BP measurements will be constrained by GRACE OBP data, and the depth-integrated external transport variability will be determined between mooring pairs from the adjusted bottom pressure. The total transport variability at 26°N compared against AMOC transport data from the RAPID project, allowing correlation and long-term trends to be analysed. The results should also allow the efficacy of using GRACE data to correct for bottom pressure sensor drift to be evaluated.

2 Background - AMOC transport calculations

AMOC transport at 26°N is estimated using the approach described in McCarthy et al. (2015), where three main components are determined from measurements and a fourth is a residual. The Gulf Stream transport (T_{GS}), which at 26°N is confined to the Florida Straits, is measured by submarine cables and calibrated by regular hydrographic sections (Meinen et al. 2010, Baringer & Larsen 2001). The Ekman transport component (T_{EK}) is calculated from reanalysis wind fields, and the baroclinic geostrophic transport, called the internal transport (T_{INT}) by the RAPID project, is determined from two different sources. Firstly, direct estimates of the flow are made by current meters between the Bahamas and 76.75°W, a component referred to as the Western Boundary Wedge (WBW). Eastwards of this longitude to the Canaries, the mid-ocean geostrophic flow is estimated from dynamic height moorings relative to a depth of no motion (usually 4820 dbar). The moorings at the western and eastern boundaries and the mid-Atlantic ridge are merged to obtain the dynamic height moorings, which are used to calculate eastern and western basin transports. The external transport (T_{EXT}), referred to hereafter as the hypsometric compensation to distinguish it from the BP-derived external transport, is an additional transport that when added to the other components gives a zero net flow at each depth across the section (Equation 1). The justification for this is that the volume of the North Atlantic above 26°N is conserved over longer timescales, as the small inputs and outputs $\mathcal{O}(1 \text{ Sv})$ are balanced. This method was initially validated by comparing the external transport determined by this method with an estimate from in-situ bottom pressure data from a single year (Kanzow et al. 2007).

$$T(z, t) = T_{GS}(z, t) + T_{EK}(z, t) + T_{INT}(z, t) + T_{EXT}(z, t) \quad (1)$$

3 Methods

3.1 Data

Bottom pressure data from RAPID mooring deployments were provided detided using harmonic fits, then filtered using a 1.625 day Tukey filter to remove the tides. This is vital as the amplitude of bottom pressure signals related to the tides are approximately an order of magnitude greater than those associated with the external transport. The sensors used by the RAPID project are accurate to better than 0.01 decibar (dbar) (Meinen et al. 2013). The mooring deployments varied in length, some early moorings had only a single deployment of around a year, however later ones had up to 8 or 9 deployments each lasting around 12 to 18 months. For this study, only two moorings each from the eastern boundary (*EB1* and *EBH1*), mid-Atlantic ridge (*MAR1* and *MAR3*) and western boundary (*WB2* and *WB4*) provided time series of sufficient length, with data from all six moorings covering the period from 18 May 2004 to 23 May 2014. The approximate mooring positions of the RAPID array are shown in Figure 1, with the western boundary moorings shown separately for clarity in Figure 2. Most deployments overlapped with the preceding and following ones, usually by 6–12 months, although a few had no overlap at all, and occasionally a deployment was missing entirely due to instrument loss or failure. Some moorings had two bottom pressure sensors deployed over the same period to allow for redundancy, while others had data from only a single sensor. Data from three deployments, one each from *WB2*, *EB1* and *MAR3* were discarded due to obvious sensor error; for the first two there were concurrent sensor data available, however the removal of the third deployment left an additional data gap. Two moorings already had significant data gaps, presumably due to sensor failure or loss: *EB1* had a gap of 139 days between 7 March 2006 and 24 July 2006, and *EBH1* had a gap of 153 days between 5 December 2005 and 5 July 2006.

The GRACE dataset used was Version 2 of the Jet Propulsion Laboratory (JPL) GRACE Mascon Equivalent Water Height RL05M.1 (Wiese et al. 2015, Watkins et al. 2015, Wiese et al. 2016), which employs a Coastal Resolution Improvement (CRI) filter that reduces leakage

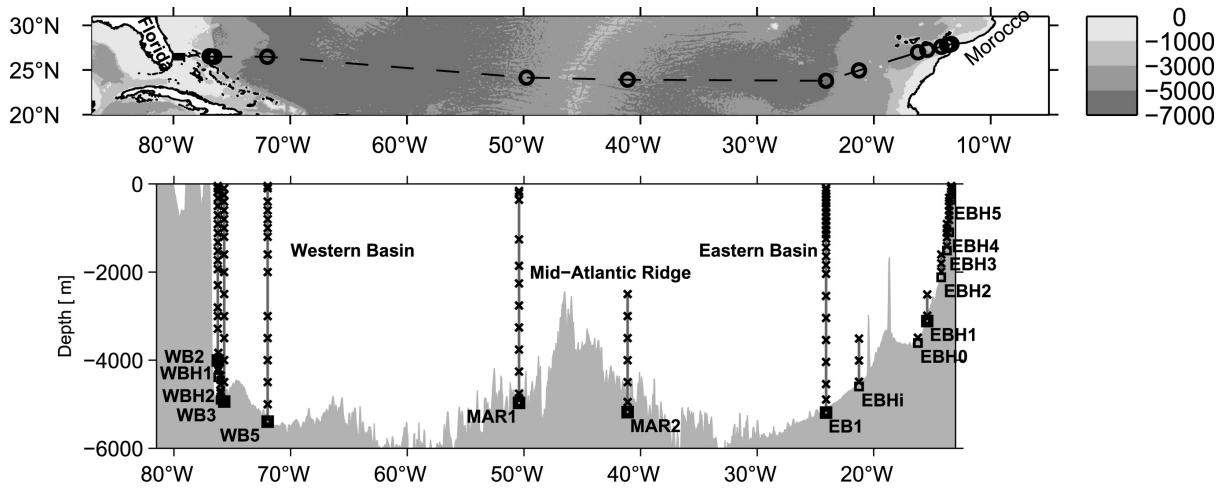


Figure 1: RAPID array: The distribution of moorings along 26.5°N in the subtropical North Atlantic as a plan view (top) and section (bottom). WB_4 is not shown but is slightly further east than WB_3 at around 26.5°N , 75.9°W . (Kanzow et al. 2010)

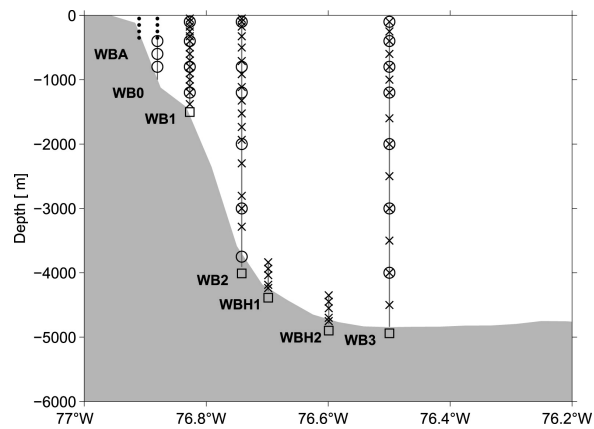


Figure 2: RAPID array: Moorings near the western boundary (off Abaco, the Bahamas). Bottom pressure recorders are shown by squares. WB_4 is not shown but is slightly further east than WB_3 at around 26.5°N , 75.9°W . (Kanzow et al. 2010)

errors when a mascon covers both land and ocean. GRACE datasets are available at <http://grace.jpl.nasa.gov>, supported by the NASA MEaSUREs Program. The JPL RL04 dataset was shown to correlate well with in-situ bottom pressure measurements by Park et al. (2008) (see section 1), and the RL05 dataset has an improved signal-to-noise ratio compared to RL04 (Chambers & Bonin 2012). Ocean bottom pressure time series derived from mascon solutions show improved correlation with in-situ data than those derived from the alternative spherical harmonic solutions, especially at lower latitudes (Watkins et al. 2015). The RL05M.1 dataset provides a liquid water equivalent (LWE) thickness in centimetres gridded to a regular 0.5 degree grid of latitude and longitude. The sampling interval is not fixed, but is approximately 30 days. Corrections for solid earth global isostatic adjustment (GIA) trends had already been made to the data following the model by A et al. (2013).

Additional data used from the RAPID program were in-situ temperature and practical salinity time series given at 20 dbar pressure intervals for individual deployments for the moorings *EB1*, *MAR1*, *MAR3*, and *WB4*. There were small data gaps of a few days between each deployment, and there were also a couple of larger gaps (approximately 1 year in length) where moorings were lost. Any data gaps longer than a few days were filled using the depth-mean temperature and salinity for the whole mooring, then the short gaps between deployments were filled by linear interpolation. The RAPID project also provided hypsometric compensation data determined relative to 4820 dbar from 02 April 2004 and 11 October 2015, and given every 20 dbar. Hypsometric compensation data both including and excluding the mid-Atlantic ridge were used, and both were integrated over the full depth. RAPID project data had already been detided with a two-day fifth-order Butterworth filter. Hydrographic data for 26°N from 2010 provided in-situ temperature, practical salinity and pressure measurements along the RAPID mooring latitude. For software, Matlab R2016b was used throughout, and additional packages used were the Gibbs Seawater (GSW) Oceanographic Toolbox (McDougall & Barker 2011) and the JLab data analysis toolbox v. 1.6.3 (Lilly 2017).

3.2 Removal of drift from bottom pressure data

Instrument drift in these bottom pressure records was observed to be most severe at the beginning of deployment, irrespective of the direction of drift, and is illustrated by two typical

mooring deployments in Figure 3. To allow a linear fit to better approximate the drift, the first 50 days of each deployment time series was removed. The overlaps described above allowed continuous time series to still be obtained for most of the moorings despite this shortening, however a 50 day gap was introduced to the *WB4* mooring between 27 April 2009 and 16 June 2006, as the two of the deployments were consecutive rather than overlapping. The lengths of both gaps in *EB1* and *EBH1* described in subsection 3.1 were also increased by 50 days.

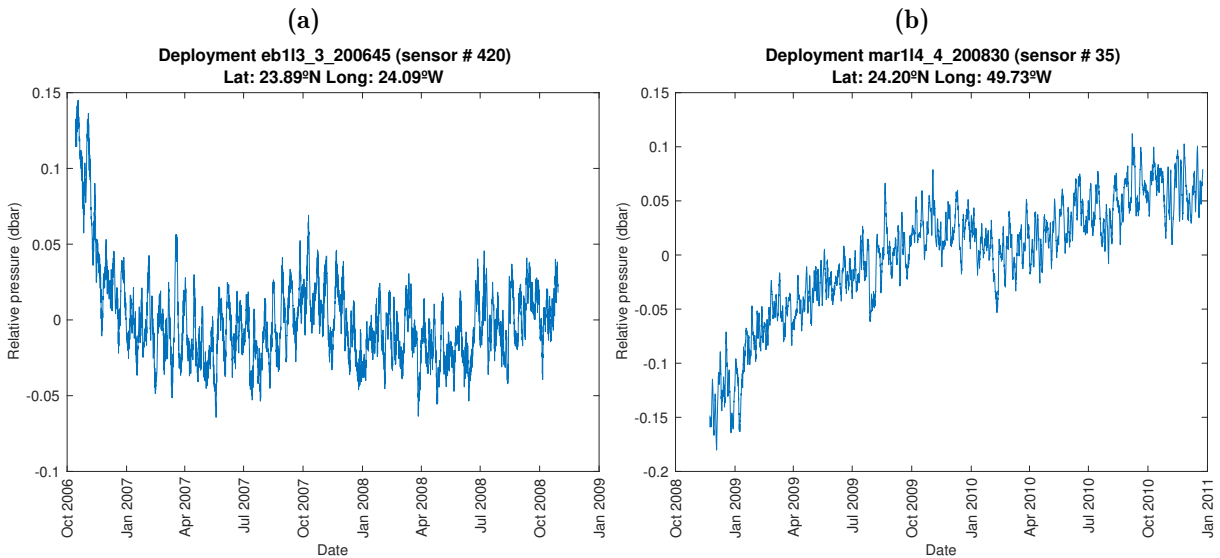


Figure 3: *Relative bottom pressures for two deployments from (a) EB1 and (b) MAR1 showing that instrument drift is typically most severe at the beginning.*

To compare GRACE and sensor data, the sensor bottom pressure (P) was converted to an equivalent water thickness in centimetres (h) using the hydrostatic balance $P = \rho gh$, where the average density ρ was estimated for each mooring longitude from hydrographic data from 26°N , and local gravity g was determined for each mooring latitude and depth. The GRACE OBP was found closest to each mooring position using the 0.5° resolution for the same period as the sensor deployment, and the sensor BP data were averaged over the same sampling time intervals as the GRACE data. The comparison of GRACE and unadjusted sensor BP records for the *WB2* mooring is shown in Figure 4a, with solid and dashed lines of the same colour representing two bottom pressure sensors deployed at the same time, and different colours showing the different deployments for the mooring. The GRACE OBP is shown by the black line. The GRACE BP was then subtracted from the sensor BP to give an approximation to the instrument drift (coloured lines), and a linear fit (dashed black line) was made to the difference (Figure 4b).

This linear fit was then subtracted from the time-averaged sensor BP to adjust for sensor drift. For deployments with two sensors, the mean post-adjustment value was used, and Figure 4c shows the comparison again of GRACE (thin black line) and sensor BP (coloured lines) for the *WB2* mooring, but now with the sensor data adjusted for sensor drift.

The original in-situ bottom pressure records were then adjusted for instrument drift by subtracting the same linear fit. Data gaps in the GRACE-adjusted time series were longer than 50 days, so were filled using a technique described by DiNezio et al. (2009), where an annual cycle based on the monthly-averaged, GRACE-adjusted bottom pressure record is modified by adding the linear fit to six months before and after the gap. Overlapping sections were first interpolated onto the same time grid, with the higher sampling frequency used if the two sections differed (Figure 5a). Since the instrument drift was generally observed to be higher at the beginning of deployments, it was assumed that the BP measurements at the end of a deployment would be more reliable than those at the start of the next. Both sections were multiplied by a weighting grid, with the grid decreasing linearly from 1 to 0 for the ending section, and increasing linearly from 0 to 1 for the beginning section (Figure 5b). The mean of the weighted sections (Figure 5c) was taken and used to replace one of the overlapping sections, and the other overlapping section removed.

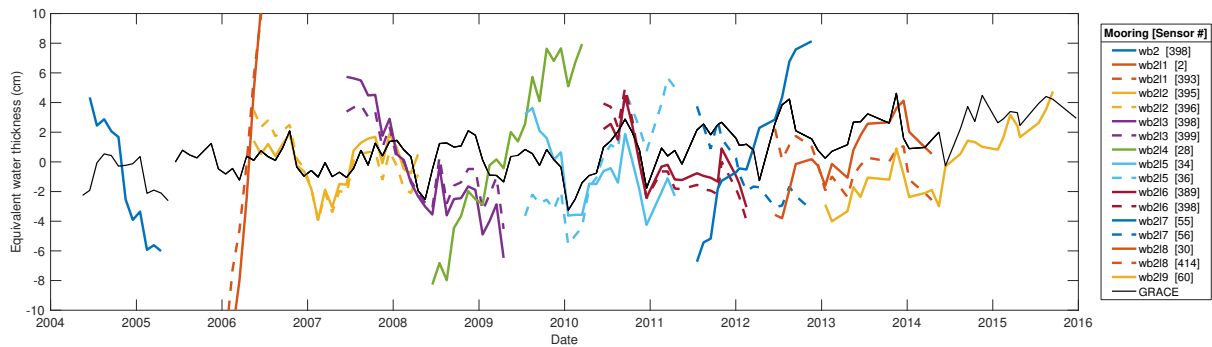
3.3 Estimation of external transport variability

Kanzow et al. (2007) describe how the vertically-integrated external transport (T'_{EXT}) fluctuations between moorings A and B can be estimated using:

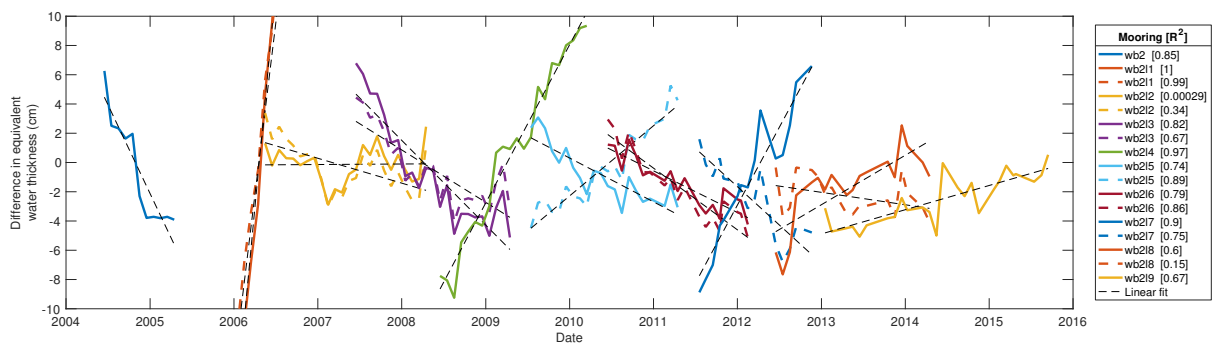
$$T'_{ext} = \frac{H}{f\rho} [P'_{bot}^A - P'_{bot}^B] \quad (2)$$

where P'_{bot} is the fluctuation in bottom pressure at a given mooring, f is the Coriolis parameter, ρ is density and H is the water column height. To use Equation 2, the complete GRACE-adjusted BP record for each mooring (e.g., *WB2* shown in Figure 6) was used to estimate the transport between pairs of moorings. For moorings of different depths, the relative pressure contribution due to density fluctuations between the shallower and deeper mooring depths was used to adjust the deeper mooring pressure.

(a) Comparison of BP (as water thickness) from individual deployment sensors (coloured lines) and GRACE (thin black line). Where two sensors were deployed together, a solid and dashed line are shown in the same colour. The sensor number is shown in brackets in the legend.



(b) The difference between BP from sensors and GRACE (coloured lines) with a linear fit to each (dashed black line), with the R^2 for the fit to each deployment shown in brackets in the legend.



(c) Comparison of GRACE-adjusted (instrument drift removed) BP from deployment sensors (coloured lines) and GRACE OBP (thin black line). Where two sensors were deployed, the mean post-adjusted value was used.

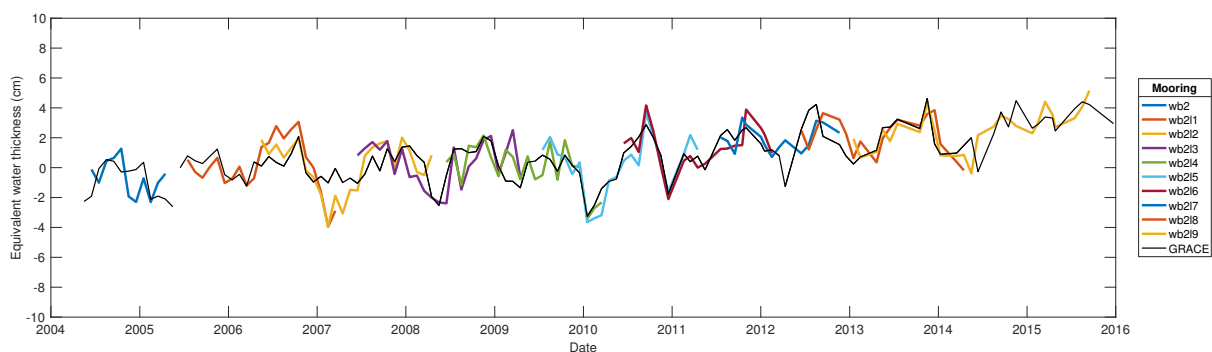
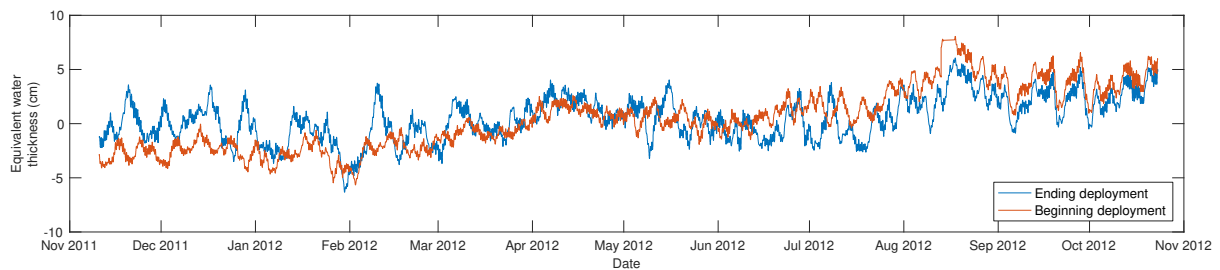
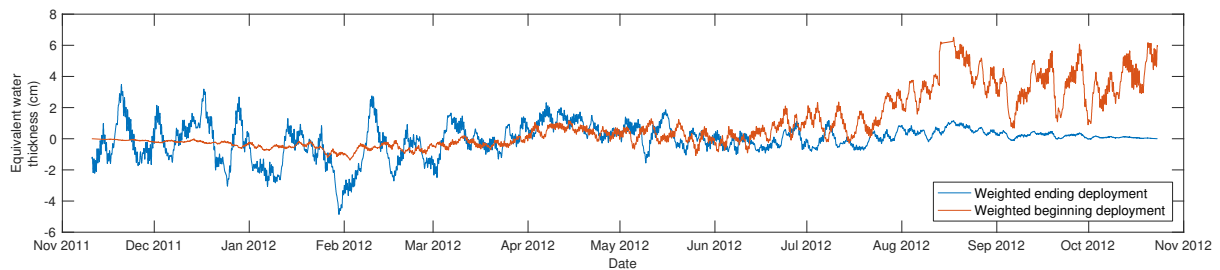


Figure 4: Using GRACE data to adjust WB2 mooring sensor data for instrument drift

(a) Unweighted overlapping sections of two EB1 mooring BP records, from deployments EB1L7 (blue) and EB1L8 (red). EB1L7 was deployed from 06 Jan 11 to 23 Oct 12, and EB1L8 from 25 Sep 11 to 24 May 14. After removal of the first 50 days, they overlapped by 348 days between 10 Nov 11 and 23 Oct 12 as shown.



(b) Overlapping sections of the two EB1 mooring deployments, EB1L7 (blue) has been multiplied by a weighting that decreases linearly from 1 to 0, and EB1L8 (red) by one that increases linearly from 0 to 1.



(c) Mean of weighted overlapping sections

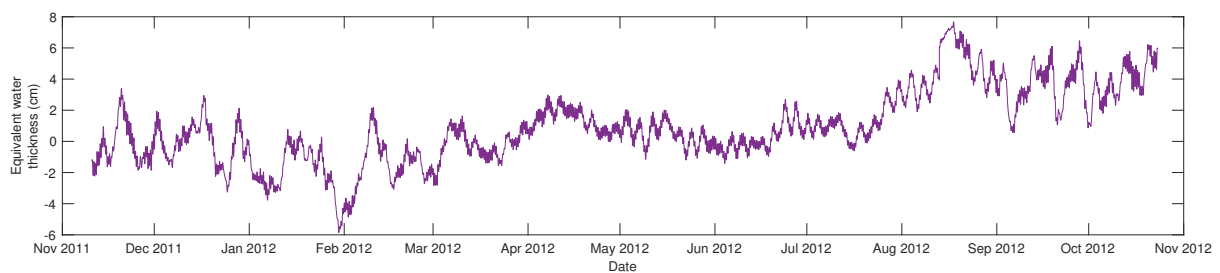


Figure 5: Replacement of overlapping sections by mean of weighed overlaps

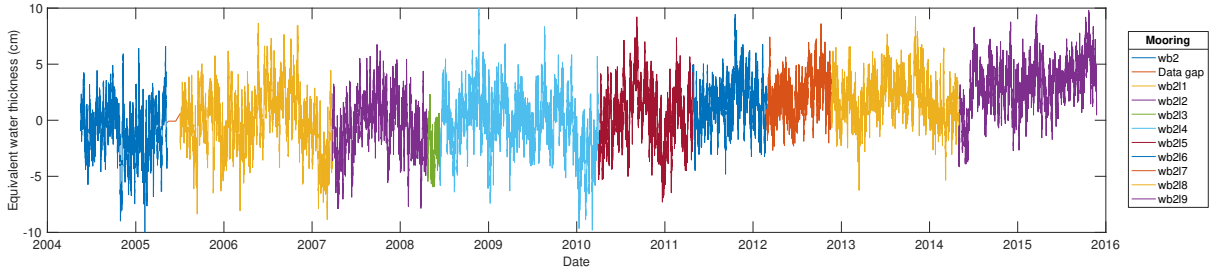


Figure 6: Complete BP (as equivalent water thickness) time series for the WB2 mooring, with instrument drift adjusted for using GRACE data and overlapping sections replaced by a weighted mean

For each deeper mooring of a pair, the in-situ temperature and practical salinity were converted to conservative temperature and absolute salinity, which were then used to obtain the steric height relative to the deeper mooring pressure using the Gibbs Seawater (GSW) Oceanographic Toolbox (McDougall & Barker 2011). Steric height was used as the BP records were in centimetres of equivalent water thickness. Ideally the pressure at the deeper mooring would be used as a reference pressure, however the temperature and salinity data for some of the moorings (*WB4* and *EB1* particularly) did not reach the full depth required. If this was the case, the deepest pressure common to all the records for a mooring was used as a reference pressure. For *MAR1* and *MAR3*, the temperature and salinity data were sufficiently deep, so the median mooring depth was used as the reference pressure. Details of the mooring depths and reference pressures used are given in Table 1. Once the steric height was determined relative to the reference pressure, the time-mean at each pressure was subtracted from it to give the steric height variability. The steric height variability at the shallower mooring depth was then added to the deeper mooring LWE thickness. For the MAR moorings, if the *MAR1-MAR3* transport component was being estimated, then the steric height variability at 3700 dbar relative to the mooring depth was determined. The rationale for this is that water exchange across the mid-Atlantic ridge occurs down to around 3700 dbar due to the presence of zonal deep fractures (Kanzow et al. 2007). If hydrostatic adjustment between moorings of different depths was done before estimating the transport variability, then the shallower mooring depth was used as H in Equation 2. If it was not done, the average of the two mooring depths was used for H .

After hydrostatically adjusting between the mooring pairs (if done), the BP as equivalent water thickness (in cm) was converted into back into pressure (in Pa) using the same mooring-specific

values for ρ and g as before, and the latitude halfway between the two moorings was used to determine the Coriolis parameter f . The transports for each mooring pair were summed to give an estimated external transport for the 26.5°N section. Two different external transports were estimated, one excluding and one including the MAR. Kanzow et al. (2007) compared the transports estimated both including and excluding the MAR transport above 3700 dbar determined from the *MAR1* and *MAR2* bottom pressure records, and found a difference in total external transport of ± 1.1 Sv. They used this result in justifying the exclusion of the MAR transport component. In this study, the same method was followed, with hydrostatically-adjusted boundary components *WB2-WB4* and *EB1-EBH1* used together with the cross-basin component *WB4-EB1*, ignoring the MAR moorings. Additionally, transport between all six mooring pairs *WB2-WB4*, *WB4-MAR1*, *MAR1-MAR3*, *MAR3-EB1* and *EB1-EBH1* was also estimated, with hydrostatic adjustment for *WB2-WB4*, *WB4-MAR1*, *MAR1-MAR3* and *EB1-EBH1* as described. *MAR3* and *EB1* were so close in depth (median depths 5055 and 5088 m respectively) that hydrostatic adjustment was not done for this pair. Unless otherwise mentioned, the first method excluding the MAR transport will be used. Finally, all component and total transport estimates and the hypsometric compensation were smoothed using a 15-day Tukey window to remove high-frequency variability. These smoothed time series are used for the comparisons in section 4.

Table 1: *Mooring depth ranges and median values, and the reference pressure used for each to determine the steric height*

Mooring	Minimum depth (m)	Maximum depth (m)	Median depth (m)	Reference pressure (dbar)
WB4	4691	4821	4752	4580
MAR1	4760	5227	5147	5147
MAR3	5041	5200	5055	5055
EB1	5000	5104	5088	4960

In order to evaluate the effectiveness of using GRACE data to adjust the mooring data from instrument drift, a linear fit was made to the instrument drift itself, so to the in-situ BP record,

rather than to the difference between the in-situ sensor BP and the GRACE BP described in subsection 3.2. The in-situ BP data was again averaged over the same time intervals as the GRACE data, and a linear fit made to each deployment. This was subtracted from the unadjusted data and a transport time series for each mooring obtained using the same methods described above.

4 Results

4.1 Correlation between external transport and hypsometric compensation

The estimated external transport, taken as the sum of the transports between the mooring pairs *WB2-WB4*, *WB4-EB1*, and *EB1-EBH1* determined from GRACE-adjusted bottom pressure differences, is shown compared to the hypsometric compensation estimated as the residual in the RAPID AMOC transport calculation in Figure 7. Both time series were detrended and smoothed using a 15-day Tukey window, and there was approximate hydrostatic adjustment for different mooring depths made. The hypsometric compensation used here ignores the mid-Atlantic ridge. The two time series show a strong correlation ($r = 0.66$, significant at the 99% level). They appear to correspond reasonably well over both shorter and longer timescales, with periods of better agreement highlighted in grey. Most strong peaks in hypsometric compensation (e.g. Dec 2007, Jan-Mar 2010, Jan 2011, Feb-Apr 2013 and Nov-Dec 2013) are matched by a similar peak in external transport, but there are two strong negative external transport peaks in May 2005 and 2006 where there is no corresponding hypsometric compensation peak. Variability of external transport is slightly greater than variability of hypsometric compensation (RMS: 10.2 vs 9.0 Sv for the detrended, smoothed time series).

Coherence between two time series tests how well they correspond at different frequencies or periods. In this case it is calculated using a multi-taper spectrum following Percival & Walden (1998), which reduces spectral leakage while minimising the data loss associated with other tapers. Figure 8 shows that the estimated external transport and hypsometric compensation are significantly coherent and in-phase for most periods between 10 and 180 days, with peaks at between 30 and 40 days, around 50 days and between 75 and 100 days. Coherence is much lower, at just above the level of significance, for periods between 180 days and 1 year. The lowest

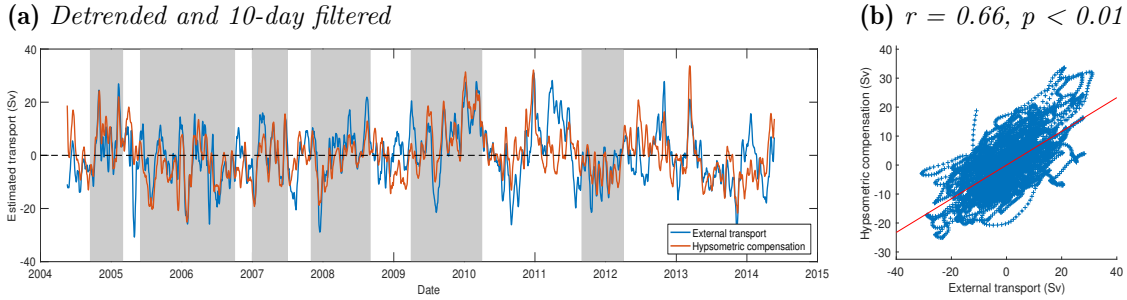


Figure 7: (a) Transport variability time series for hypsometric compensation (red) and the estimated external transport (blue), with a dashed line marking zero. Grey areas highlight periods of stronger agreement between the two. (b) Scatter plot for the same data showing correlation coefficient r , with a red line showing the best linear fit. Both time series were detrended and smoothed with a 15-day Tukey window.

coherence is at just over 180 days, and corresponds to the two time series being out of phase by around 30° , equivalent to a lag of about 15 days for a 180 day period. For periods longer than a year, the coherence between external transport and hypsometric compensation increases and is in phase again. The same two time series are further smoothed with a 30-day Tukey window as a result of the significant coherence at 30 to 40 days, which shows the agreement between them more clearly (Figure 9). The correlation following the increased smoothing is still strong ($r = 0.62$, significant at the 99% level).

The relative contribution of each mooring pair to the total external transport anomaly is shown in Figure 10, with each component offset by 100 Sv to allow clear comparison. The correlations between each component and the hypsometric compensation (bottom plot) are very weak ($r < 0.25$) and not significant at the 90% level, especially compared to the stronger correlation ($r = 0.66$) between the total transport and the hypsometric compensation. The component that correlates least weakly with the hypsometric compensation is the main basin, WB_4-EB1 ($r = 0.23$), although it is not significant at the 90% level. The western and eastern boundary components, WB_2-WB_4 and $EB1-EBH1$, show the weakest correlations ($r = 0.064$ and 0.11 respectively). The greatest variability is shown by the mooring pair transports of WB_2-WB_4 and WB_4-EB1 (Figure 11), but they also show a strong inverse relationship, and appear to largely offset each other. This is illustrated in Figure 12, which indicates a very strong inverse correlation ($r = -0.90$, significant at the 99% level) between the two transports, and significant

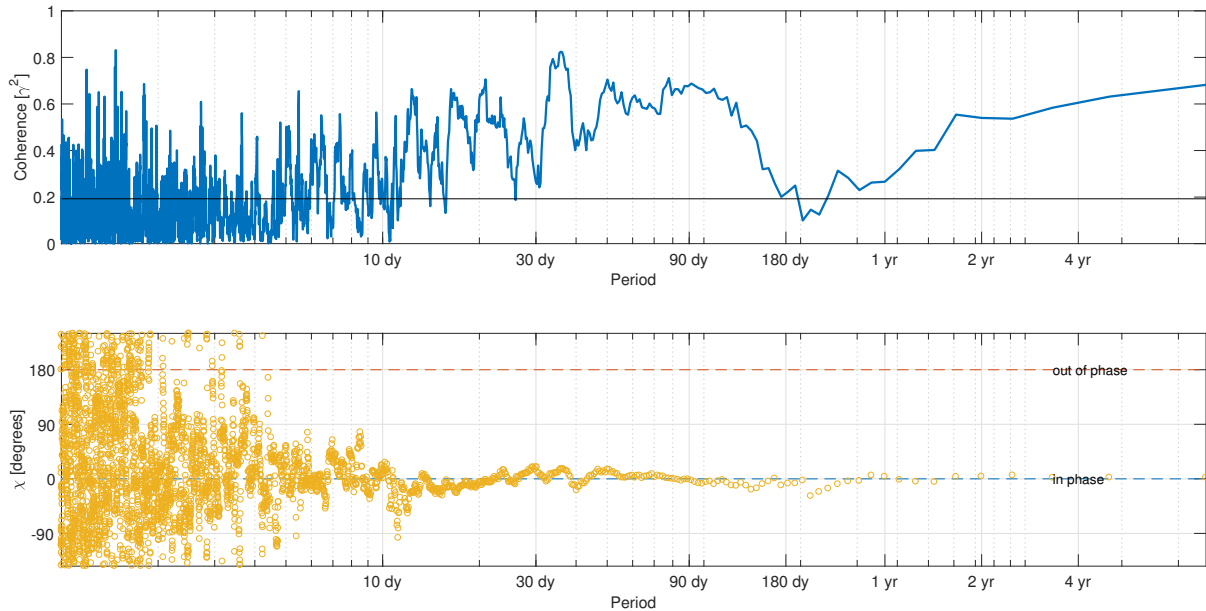


Figure 8: Coherence between estimated external transport and hypsometric compensation (both detrended and smoothed with a 15-day Tukey window). The upper figure shows coherence, with significance indicated by the horizontal black line. The lower figure shows the phase relationship for the same period.

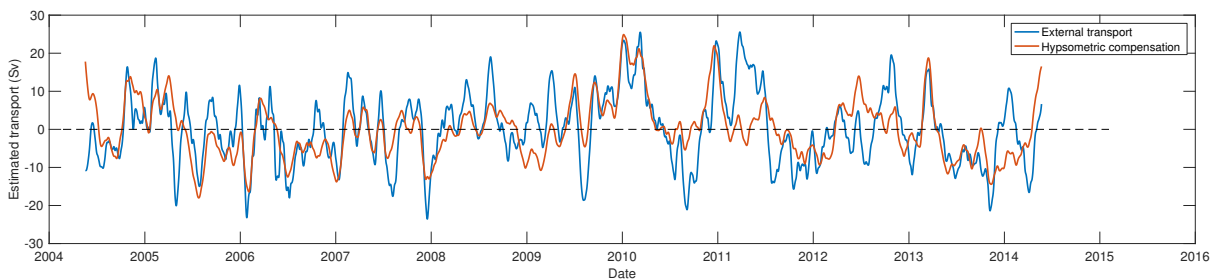


Figure 9: Transport variability time series for hypsometric compensation (red) and the estimated external transport (blue), with a dashed line marking zero. Both time series were detrended and smoothed with a 30-day Tukey window.

out-of-phase coherence (Figure 12b) between all variability on timescales greater than a month, shown by the periods above the significance limit in the bottom figure of Figure 12b.

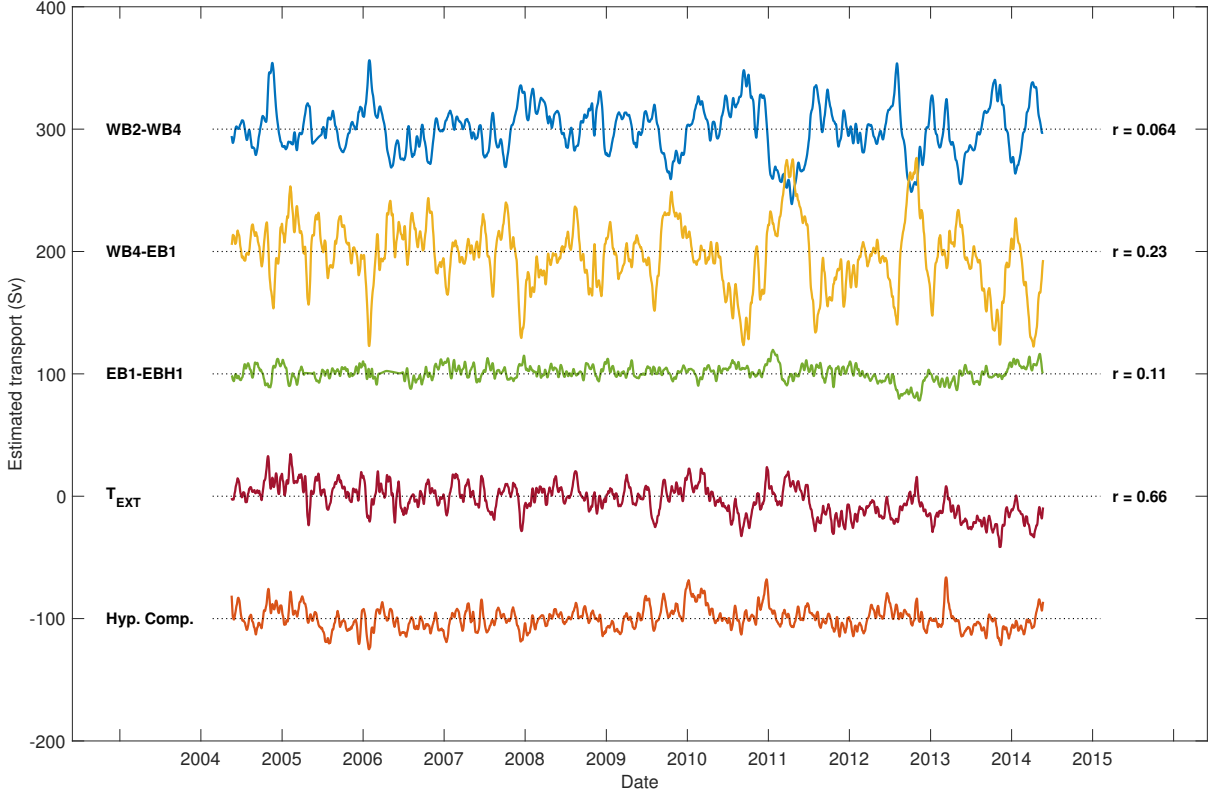


Figure 10: *Estimated transport variability between each mooring pair compared with the total estimated transport, with the correlation coefficient between the mooring pair transport and the hypsometric compensation shown for each (each component is offset by 100 Sv for clarity and the zero transport marked with a dotted line). All time series were detrended and smoothed with a 15-day Tukey window.*

4.2 Evaluation of using GRACE data

The effectiveness of using GRACE bottom pressure data to adjust for instrument drift is examined by comparing both T_{EXT} derived using the linear fit to the sensor record itself and T_{EXT} derived using the linear fit to the difference between the GRACE and deployment LWE (as described in subsection 3.2). The correlation between the external transport using the ‘fit-to-record’ method and hypsometric compensation is only moderate ($r = 0.52$, significant at the 99% level) (Figure 13b), compared with the stronger correlation ($r = 0.66$) using the

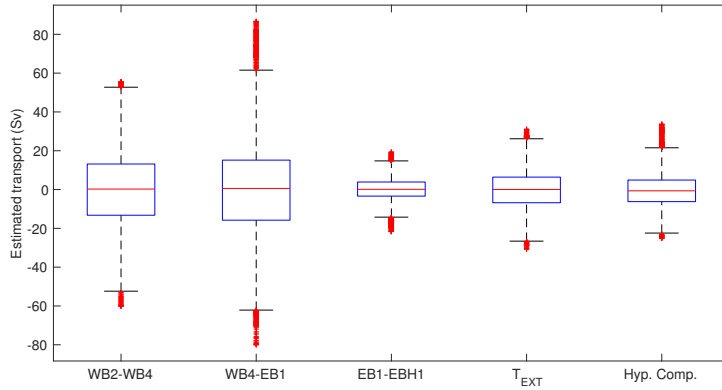


Figure 11: Boxplot showing median, 25th and 75th percentile and range of transport variability for each mooring pair transport, the total external transport T_{EXT} , and the hypsometric compensation.

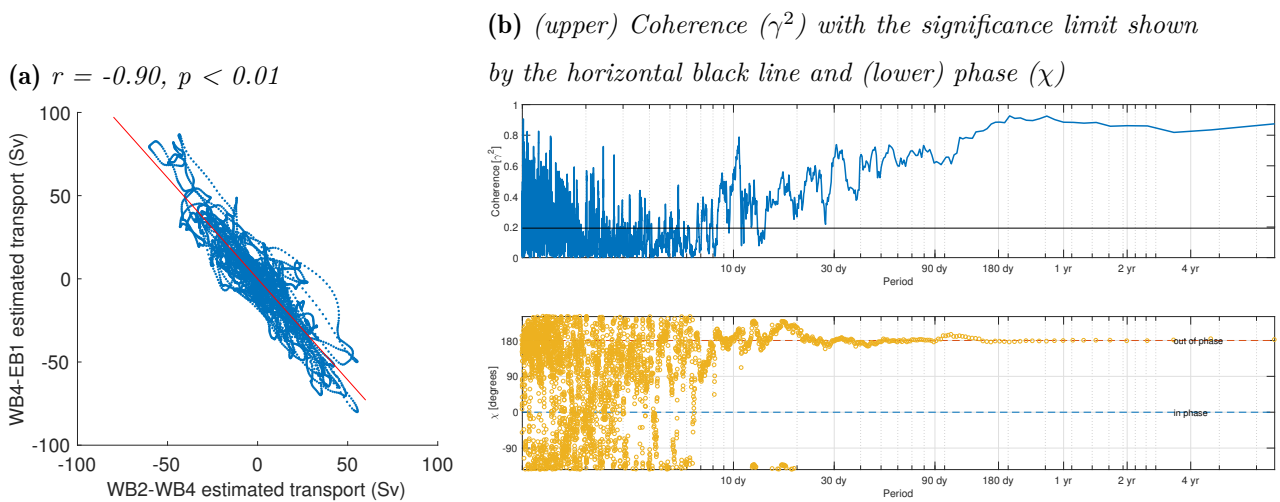
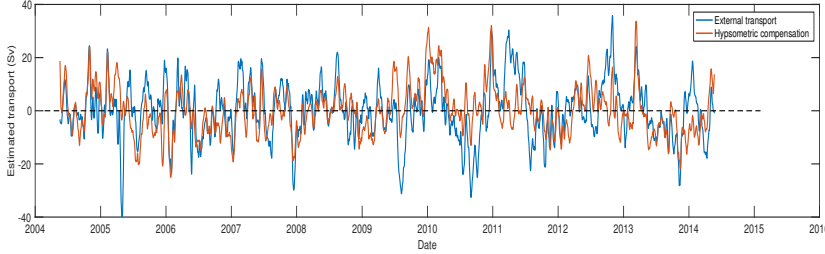


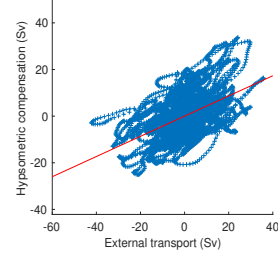
Figure 12: (a) Correlation, with the best linear fit shown by a red line and (b) Coherence between estimated transport variation for WB2-WB4 and WB4-EB1 mooring pairs

GRACE-adjusted method (Figure 13d).

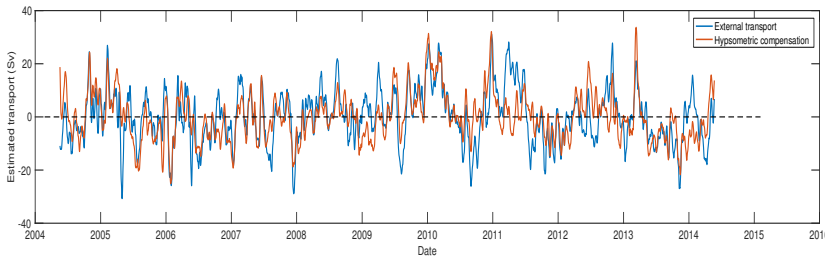
(a) *Sensor drift adjusted using linear fit to sensor drift*



(b) $r = 0.52, p < 0.01$



(c) *Sensor drift adjusted using linear fit to difference between sensor and GRACE data*



(d) $r = 0.67, p < 0.01$

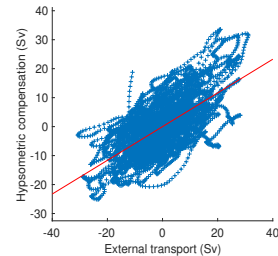


Figure 13: Comparison of methods to adjust BP for sensor drift: (a) and (c) Time series for hypsometric compensation (red) and the T_{EXT} (blue), with a dashed line marking zero anomaly. (b) and (d) Scatter plots for the same data showing correlation coefficient r , with the red line showing the best linear fit.

The agreement between GRACE OBP and the GRACE-adjusted sensor BP record varies between the moorings; the two moorings with the highest and lowest correlation between the two time series are shown in Figure 14, with error bars showing the reported uncertainty of the GRACE OBP data. The BP variability derived from the sensor data at *WB2* shows a strong correlation with the GRACE OBP data for the closest mascon ($r = 0.67$ significant at the 99% level, Figure 14b), and is well within the uncertainty (Figure 14a), whereas the BP variability at *EBH1* shows almost no correlation with the corresponding GRACE data ($r = 0.02$, Figure 14d) and frequently exceeds the GRACE BP uncertainty (Figure 14c). Correlation between the remaining mooring BP records and the OBP from the nearest GRACE mascon is weak to moderate (*WB4* ($r = 0.26$), *MAR3* ($r = 0.31$), *MAR1* ($r = 0.40$), to *EB1* ($r = 0.45$)).

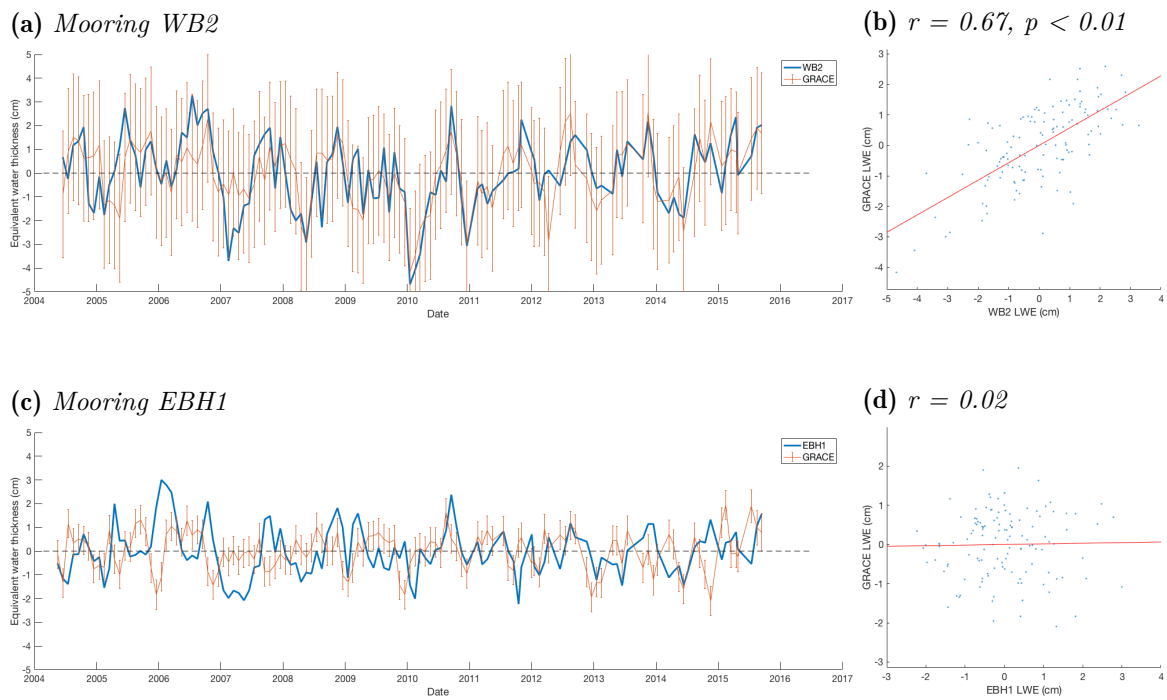


Figure 14: Comparison of monthly-averaged BP (as equivalent water thickness) from mooring sensors and GRACE: (a) and (c) BP time series from GRACE (red) and mooring sensor (blue), with a dashed line marking zero, error bars show the uncertainty of the GRACE equivalent water thickness (cm). (b) and (d) Scatter plots for the same data showing correlation coefficient r and significance, with the red line indicating the best linear fit.

4.3 Evaluation of including mid-Atlantic ridge transport

To compare the effect of including the mid-Atlantic ridge mooring BP data to estimate external transport, the transport between mooring pairs $WB2-WB4$, $WB4-MAR1$, $MAR1-MAR3$, $MAR3-EB1$ and $EB1-EBH1$ was estimated. The total external transport as the sum of these five components was compared to hypsometric compensation including the MAR, and both were smoothed using a 15-day Tukey filter and detrended as before. The correlation between them is also strong ($r = 0.64$, significant at the 99% level), very similar to the correlation between hypsometric compensation and T_{EXT} excluding the MAR ($r = 0.66$).

Although the two methods give similar results when the total external transport is compared, one advantage of using this method is that we can look at variability within the separate western and eastern basin transport components and the MAR component Figure 16. Again, none of the transport components dominates the external transport, and all are weakly correlated with the hypsometric compensation. The components with the least weak correlation with the hypsometric compensation are the main western and eastern basins, $WB4-MAR1$ and $MAR3-EB1$ ($r = 0.17$ and 0.22 respectively). The western boundary component, $WB2-WB4$, has the weakest correlation ($r = 0.078$) and the Mid-Atlantic Ridge component, $MAR1-MAR3$ and eastern boundary component $EB1-EBH1$ are both correlated weakly ($r = 0.11$) with the hypsometric compensation. The greatest variability is shown by the mooring pair transports of $WB2-WB4$ and $WB4-MAR1$ (Figure 15), but they show a strong inverse relationship similar to $WB2-WB4$ and $WB4-EB1$ in subsection 4.1 when the MAR component is not included, and also appear to largely offset each other.

This approach also allows us to compare the western and eastern transport components, as the sum of $WB2-WB4 + WB4-MAR1$ for the western component, and $MAR3-EB1 + EB1-EBH1$ for the eastern component (Figure 17). The correlation between the western transport component and the external transport is much stronger than that of the eastern transport component ($r = 0.77$ compared to $r = 0.17$, both significant at the 99% level). It also appears that the western component was the primary contributor to the large peaks in the total external transport between 2009 and 2010 and in 2011, and to a slightly lesser extent to the peaks in late 2012 and 2013.

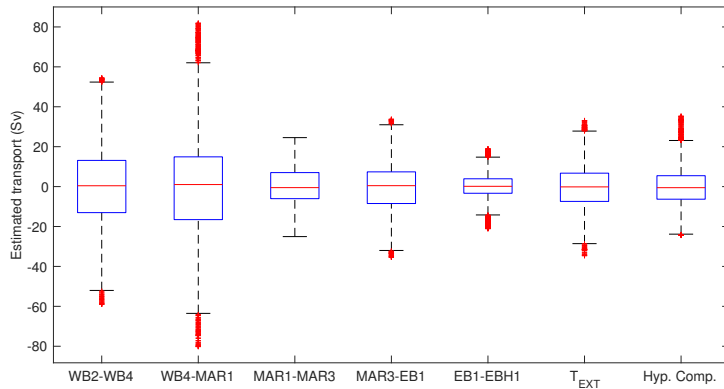


Figure 15: Boxplot showing median, 25th and 75th percentile and range of transport variability for each mooring pair transport, the total external transport T_{EXT} , and the hypsometric compensation.

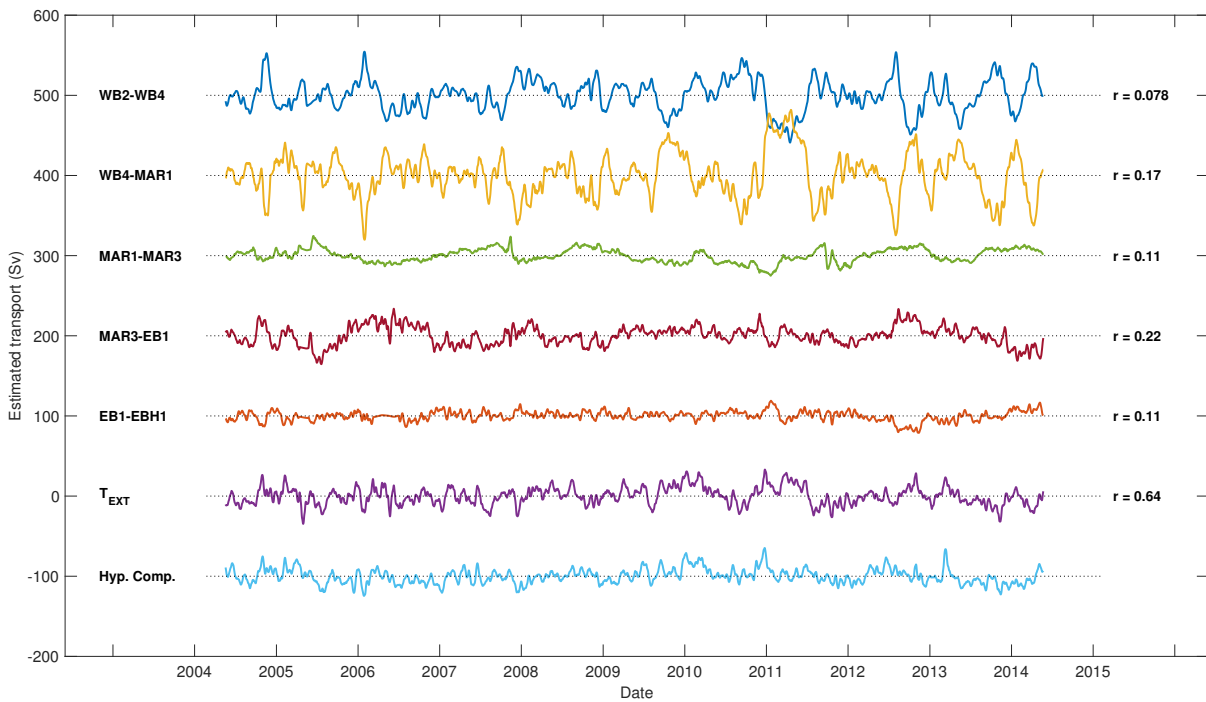


Figure 16: Estimated transport variability between each mooring pair compared with the total estimated transport (each component is offset by 100 Sv for clarity and the zero transport marked with a dotted line). All time series are detrended and smoothed with a 15-day Tukey window.



Figure 17: *Estimated transport variability for the western ($WB2-WB_4 + WB_4-MAR1$) and eastern ($MAR3-EB1 + EB1-EBH1$) transport components and the total external transport T_{EXT} . Each component is offset by 100 Sv for clarity and the zero transport marked with a dotted line, and all time series are detrended and smoothed with a 15-day Tukey window.*

4.4 Trend over 10 years

The external transport variability (T_{EXT}) estimated from bottom pressure is shown compared to the hypsometric compensation in Figure 18, where both time series were smoothed as before but neither were detrended. The external transport was derived from GRACE-adjusted BP records and hydrostatically adjusted for different depths between mooring pairs. Neither T_{EXT} nor the hypsometric compensation include the mid-Atlantic Ridge. A simple linear fit to both time series shows the external transport as a strengthening southward flow during the entire period, whereas the southward flow of the hypsometric compensation becomes increasingly weaker. T_{EXT} also appears to be predominantly northward during the first two years of the record, which is physically unlikely, as it would imply a net northward flow across $26^\circ N$ when combined with the other AMOC components.

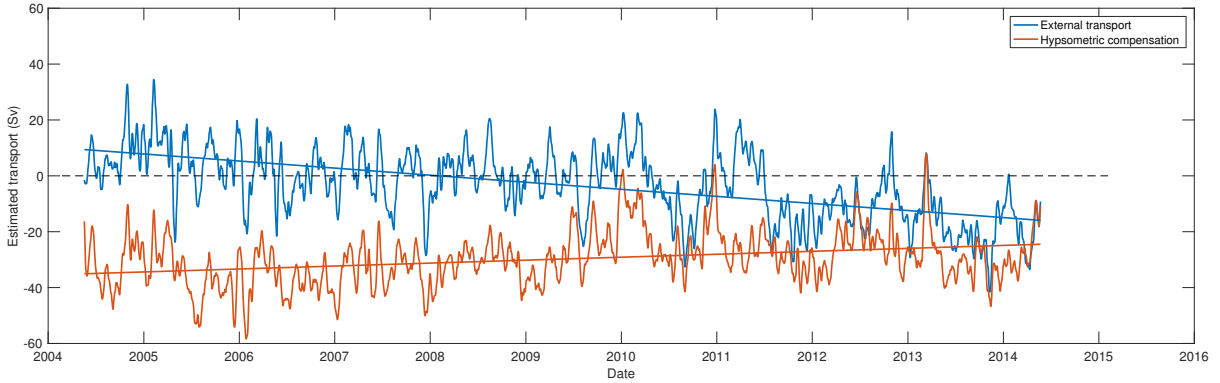


Figure 18: *GRACE-adjusted BP-derived external transport T_{EXT} (blue) and hypsometric compensation (red), showing the linear fit to each. Both time series are smoothed with a 15-day Tukey window, but are not detrended. The dotted line marks zero transport.*

5 Discussion

The GRACE-adjusted, bottom pressure-derived external transport variability and the RAPID-estimated hypsometric compensation show strong correlation ($r = 0.66$, $p < 0.01$) and significant in-phase coherence over timescales between 10 and 180 days and greater than a year, but weaker coherence over timescales between 180 days and one year. The agreement between T_{EXT} and hypsometric compensation is qualitatively comparable to the agreement ($r = 0.82$) found by Kanzow et al. (2007) between the AMOC transport variability determined using the bottom pressure-derived external transport and the RAPID residual method, when both were integrated to 1000 dbar. However the time series evaluated here are a decade long, compared with the single year records used by Kanzow et al. (2007). Kanzow et al. (2007) also found that for a single year (March 2004 to March 2005), T_{EXT} showed weak negative correlation ($r = -0.32$) with T_{EK} , which is close to the value ($r = -0.38$, $p < 0.01$) found for this longer time-series. McCarthy et al. (2012) identified a weakening in the deep southward return flow between early 2009 and mid-2010, which is seen in the increased northward T_{EXT} anomaly, and is also a period when the agreement with the hypsometric compensation is particularly good. The strong wind event of early 2013 is also represented well by T_{EXT} , and in general strong peaks in hypsometric compensation are matched with strong peaks in T_{EXT} , although the converse is not always true; strong peaks in T_{EXT} are not always matched by strong hypsometric compensation peaks. From the external transport estimate including the mid-Atlantic (MAR) contribution, we can

see that the western (*WB2-MAR1*) component appears to be the primary contributor to strong peaks such as the 2009–2010 weakening event.

The mooring pair transport components when the MAR is excluded show that no single component dominates the total external transport, and that variability is highest (RMS: 27.9 Sv) for the main basin component (*WB4-EB1*), although this is strongly negatively correlated ($r = -0.90$, $p < 0.01$) with the western boundary component (*WB2-WB4*) over all time scales. The overall effect of this anti-correlation between *WB2-WB4* and *WB4-EB1* transport variability is that the western boundary transport would have offset a significant part of the larger basin transport. When the MAR is included, variability is highest for the western boundary (*WB2-WB4*) and western basin transport (*WB4-MAR1*) components (RMS: 20.2 and 27.6 Sv respectively for the 15-day filtered transport) and lowest for the eastern boundary transport component (RMS: 6.1 Sv). The western boundary and western basin components also show a very strong negative correlation ($r = -0.91$, $p < 0.01$) over all time scales, with the western boundary component again offsetting a significant part of the larger western basin transport. The negative correlation described for transports both excluding and including the MAR appears to be driven by high variability at the *WB4* mooring (RMS: 4.1 cm) compared to *WB2*, *EB1*, and *MAR1* (RMS: 2.8, 2.2 and 2.1 cm respectively), so that the pressure differences and thus geostrophic transport to the west and east of *WB4* will be in opposing directions.

The main driving process of T_{EXT} variability at the western boundary is likely to be variability of the deep western boundary current (DWBC) transport, which is at 26.5°N is found along the continental slope. The variability of the DWBC transport is much greater than that of the AMOC transport (standard deviations of 16 Sv compared to 5 Sv), with baroclinic and especially barotropic flows showing variability exceeding 10 Sv on timescales of days to months (Meinen et al. 2013). The time-mean eastern edge of the DWBC ‘core’ (southward current speed $> 10 \text{ ms}^{-1}$) is found at the approximate longitude of the *WB4* mooring at around 76°W (Figure 4, Bryden et al. (2005)), although it was observed to reach beyond 75.5°W during June 1990 (Figure 10, Lee et al. (1996)), so it is likely that it meanders about its time-mean position and across the *WB4* mooring position. Meinen et al. (2013) found that bottom pressure-derived transports between mooring pairs *C-D* and *D-E* deployed at 26.5°N as part of the NOAA Western Boundary Time Series were anti-correlated ($r = -0.50$). Mooring *C* is between *WB2*

and WB_4 , and D and E are east of WB_4 , so at and beyond the edge of the time-mean DWBC position. Meinen et al. (2013) attributed the anti-correlation of the mooring pair transports to meandering of the DWBC, due to the absence of lag in the correlation. It seems likely that variability of BP at WB_4 is due to variability of transport and/or position of the DWBC, but without comparing it to the relevant data it is impossible to say which, if either, is the main cause.

The generally good agreement between the GRACE-adjusted BP-derived external transport and the hypsometric compensation shows that using GRACE to adjust in-situ BP records for instrument drift is effective, despite the correlation between the actual GRACE-adjusted BP records and GRACE OBP data varying significantly, from $r = 0.26$ for WB_4 to $r = 0.67$ for WB_2 . WB_2 and WB_4 use the same GRACE mascon to provide OBP data, as it is the closest to both moorings. In this case, the coarse resolution of the GRACE data may result in the varying results of using it to adjust the in-situ bottom pressure for these two moorings. ‘Leakage’ due to steep topography seems unlikely to be the cause on the western boundary of the RAPID array, as WB_2 is closer to the continental slope than WB_4 . Leakage may still be an issue for the eastern boundary and MAR moorings, since all are close to relatively rapidly changing gradients. Landerer et al. (2015) used a Gaussian averaging filter of 50 km half width to smooth the transitions between mascons, which may improve the results for moorings close to the edge of a mascon.

When the GRACE-adjusted external transport variability is examined without the overall trend removed, a simple linear fit suggest that the southward flow is strengthening over time. This is in opposition to the weakening southward flow of the hypsometric compensation shown here and described by Smeed et al. (2014). This unexpected trend may be due to the GRACE data having a low frequency trend of its own that is introduced to the mooring bottom pressure data during the adjustment process. There are known long period signals within GRACE data that are not removed during processing, for example, components of the pole tide that have inter-annual and decadal periods (Wahr J. & Bettadpur 2015). There may also be uncertainties in GRACE trend correction for global isostatic adjustment (GIA) and land leakage, which were sufficient for Landerer et al. (2015) to leave out any trend analysis when they compared GRACE OBP-derived LNADW variability to RAPID AMOC observations. Although the GRACE data

clearly has some issues, its global, long-term coverage (due to be continued with the GRACE Follow-On mission from early 2018) make it valuable and worth using further.

6 Conclusions

This study shows that GRACE OBP data can be used to remove instrument drift from in-situ bottom pressure sensor records more effectively than a linear fit to the record itself, and allows the retention of low frequency BP variations. When instrument drift is removed from in-situ BP records from the RAPID array at 26°N using GRACE data, and external (barotropic) transport is estimated from the adjusted BP data, this external transport is correlated ($r = 0.66$, $p < 0.01$) with the hypsometric compensation from the RAPID AMOC calculation when both are detrended, and is significantly coherent at most timescales. This strong correlation provides independent verification for the AMOC transport estimation method currently used by the RAPID project.

The trend of the external transport estimated using GRACE-adjusted BP data shows a strengthening southward flow over 10 years, in opposition to that of the hypsometric compensation. This could be due to a trend within the GRACE data itself, such as long period earth tide components, that are currently not removed during processing of GRACE data. A possible next step could be to remove the pole tide components from the post-processed GRACE data, as done by Landerer et al. (2015) and repeat the study. It may also be worth trying an alternative to the linear fit to the difference between GRACE and in-situ bottom pressure records, such as an exponential-linear fit, as the goodness of the linear fit is highly variable between records. The unexpected trend seen in T_{EXT} means the study has not provided additional evidence of an AMOC slowdown, but has provided a verification of the RAPID AMOC calculation using data from a full decade.

References

A, G., Wahr, J. & Zhong, S. (2013), ‘Computations of the viscoelastic response of a 3-D compressible Earth to surface loading: an application to Glacial Isostatic Adjustment in Antarc-

- tica and Canada’, *Geophysical Journal International* **192**(2), 557–572.
- Baringer, M. & Larsen, J. (2001), ‘Sixteen years of Florida Current transport at 27 degrees N’, *GEOPHYSICAL RESEARCH LETTERS* **28**(16), 3179 – 3182.
- Bingham, R. J. & Hughes, C. W. (2008), ‘Determining North Atlantic meridional transport variability from pressure on the western boundary: A model investigation’, *Journal of Geophysical Research: Oceans (1978–2012)* **113**(C9).
- Bryden, H., Saunders, P. & Johns, W. (2005), ‘Deep western boundary current east of Abaco: Mean structure and transport.’, *Journal of Marine Research* **63**(1), 35–57.
- Chambers, D. P. & Bonin, J. A. (2012), ‘Evaluation of Release-05 GRACE time-variable gravity coefficients over the ocean’, *Ocean Science* **8**(5), 859–868.
- DiNezio, P. N., Gramer, L. J., Johns, W. E., Meinen, C. S. & Baringer, M. O. (2009), ‘Observed Interannual Variability of the Florida Current: Wind Forcing and the North Atlantic Oscillation’, *Journal of Physical Oceanography* **39**(3), 721–736.
- Jackson, L. C., Kahana, R., Graham, T., Ringer, M. A., Woollings, T., Mecking, J. V. & Wood, R. A. (2015), ‘Global and European climate impacts of a slowdown of the AMOC in a high resolution GCM.’, *Climate Dynamics* **45**(11), 3299–3316.
- Johns, W., Baringer, M., Beal, L., Cunningham, S., Kanzow, T., Bryden, H., Hirschi, J., Marotzke, J., Meinen, C., Shaw, B. & Curry, R. (2011), ‘Continuous, Array-Based Estimates of Atlantic Ocean Heat Transport at 26.5 degrees N.’, *JOURNAL OF CLIMATE* **24**(10), 2429 – 2449.
- Johns, W. E., Kanzow, T. & Zantopp, R. (2005), ‘Estimating ocean transports with dynamic height moorings: An application in the Atlantic Deep Western Boundary Current at 26 °N’, *Deep Sea Research Part I: Oceanographic Research Papers* **52**(8), 1542 – 1567.
- Kanzow, T., Cunningham, S. A., Johns, W. E., Hirschi, J. J.-M., Marotzke, J., Baringer, M. O., Meinen, C. S., Chidichimo, M. P., Atkinson, C., Beal, L. M., Bryden, H. L. & Collins, J. (2010), ‘Seasonal Variability of the Atlantic Meridional Overturning Circulation at 26.5 °N’, *Journal of Climate* **23**(21), 5678–5698.

- Kanzow, T., Cunningham, S. A., Rayner, D., Hirschi, J. J.-M., Johns, W. E., Baringer, M. O., Bryden, H. L., Beal, L. M., Meinen, C. S. & Marotzke, J. (2007), ‘Observed Flow Compensation Associated with the MOC at 26.5°N in the Atlantic’, *Science* **317**(5840), 938–941.
- Landerer, F., Wiese, D., Bentel, K., Boening, C. & Watkins, M. (2015), ‘North Atlantic meridional overturning circulation variations from GRACE ocean bottom pressure anomalies.’, *Geophysical Research Letters* **42**(19), 8114–8121.
- Lee, T. N., Johns, W. E., Zantopp, R. J. & Fillenbaum, E. R. (1996), ‘Moored Observations of Western Boundary Current Variability and Thermohaline Circulation at 26.5° in the Subtropical North Atlantic’, *Journal of Physical Oceanography* **26**(6), 962–983.
- Lilly, J. M. (2017), ‘jLab: A data analysis package for Matlab, v. 1.6.3’, <http://www.jmlilly.net/jmlsoft.html>.
- McCarthy, G., Frajka-Williams, E., Johns, W. E., Baringer, M. O., Meinen, C. S., Bryden, H. L., Rayner, D., Duchez, A., Roberts, C. & Cunningham, S. A. (2012), ‘Observed interannual variability of the Atlantic meridional overturning circulation at 26.5°N’, *Geophysical Research Letters* **39**(19).
- McCarthy, G., Smeed, D., Johns, W., Frajka-Williams, E., Moat, B., Rayner, D., Baringer, M., Meinen, C., Collins, J. & Bryden, H. (2015), ‘Measuring the Atlantic Meridional Overturning Circulation at 26°N’, *Progress in Oceanography* **130**, 91 – 111.
- McDougall, T. & Barker, P. (2011), *Getting started with TEOS 10 and the Gibbs Seawater (GSW) Oceanographic Toolbox*, SCOR/IAPSO WG127.
- Meinen, C. S., Baringer, M. O. & Garcia, R. F. (2010), ‘Florida Current transport variability: An analysis of annual and longer-period signals.’, *Deep-Sea Research Part I* **57**, 835 – 846.
- Meinen, C. S., Johns, W. E., Garzoli, S. L., van Sebille, E., Rayner, D., Kanzow, T. & Baringer, M. O. (2013), ‘Variability of the Deep Western Boundary Current at 26.5°N during 2004–2009’, *Deep Sea Research Part II: Topical Studies in Oceanography* **85**, 154 – 168. Modern Physical Oceanography and Professor H.T. Rossby.

- Park, J., Watts, D. R., Donohue, K. A. & Jayne, S. R. (2008), ‘A comparison of in situ bottom pressure array measurements with GRACE estimates in the Kuroshio Extension’, *Geophysical Research Letters* **35**(17).
- Percival, D. B. & Walden, A. T. (1998), *Spectral Analysis for Physical Applications : Multitaper and Conventional Univariate Techniques.*, Cambridge ; New York : Cambridge University Press, 1998.
- Rhines, P., Hakkinen, S. & Josey, S. (2008), *Is oceanic heat transport significant in the climate system?*, Springer Verlag.
- Smeed, D. A., McCarthy, G. D., Cunningham, S. A., Frajka-Williams, E., Rayner, D., Johns, W. E., Meinen, C. S., Baringer, M. O., Moat, B. I., Ducez, A. & Bryden, H. L. (2014), ‘Observed decline of the Atlantic meridional overturning circulation 2004 - 2012’, *Ocean Science* **10**(1), 29–38.
- Wahr J., R. S. N. & Bettadpur, S. V. (2015), ‘The pole tide and its effect on GRACE time-variable gravity measurements: Implications for estimates of surface mass variations.’, *J. Geophys. Res. Solid Earth* **120**, 4597–4615.
- Watkins, M. M., Wiese, D. N., Yuan, D., Boening, C. & Landerer, F. W. (2015), ‘Improved methods for observing Earth’s time variable mass distribution with GRACE using spherical cap mascons’, *Journal of Geophysical Research: Solid Earth* **120**(4), 2648–2671.
- Watts, D. & Kontoyiannis, H. (1990), ‘Deep-Ocean Bottom Pressure Measurement - Drift Removal and Performance’, *JOURNAL OF ATMOSPHERIC AND OCEANIC TECHNOLOGY* **7**(2), 296 – 306.
- Wiese, D. N., Landerer, F. W. & Watkins, M. M. (2016), ‘Quantifying and reducing leakage errors in the JPL RL05M GRACE mascon solution.’, *Water Resources Research* **52**(9), 7490–7502.
- Wiese, D., Yuan, D.-N., Boening, C., Landerer, F. & Watkins, M. (2015), ‘JPL GRACE Mascon Ocean, Ice, and Hydrology Equivalent Water Height JPL RL05M.1. Ver. 1. PO.DAAC,CA,USA.’, Dataset accessed [2017-01-30] at <http://dx.doi.org/10.5067/TEMSC-OCL05>.